Published in final edited form as:

FASEB J. 2020 July ; 34(7): 8902–8919. doi:10.1096/fj.202000545R.

TOK channels use the two gates in classical K^+ channels to achieve outward rectification

Anthony Lewis[1], **Zoe A. McCrossan**[2], **Rían W. Manville**[3], **M. Oana Popa**[4], **Luis G. Cuello**[5], **Steve A. N. Goldstein**[6]

[1]School of Pharmacy and Biomedical Sciences, University of Portsmouth, Portsmouth, UK

[2]NIHR Evaluation, Trials and Studies Coordinating Centre (NETSCC), University of Southampton, Southampton, UK

[3]School of Pharmacy and Biomolecular Sciences, University of Brighton, Brighton, UK

[4]Sussex Drug Discovery Centre, School of Life Sciences, University of Sussex, Brighton, UK

[5]Department of Cell Physiology and Molecular Biophysics, Center for Membrane Protein Research, Texas Tech University Health Sciences Center, Lubbock, TX 79430, USA

[6]Departments of Physiology & Biophysics and Pediatrics, School of Medicine, Samueli College of Health Sciences, University of California, Irvine, Irvine, CA, USA

Abstract

TOKs are outwardly rectifying K^+ channels in fungi with two pore-loops and eight transmembrane spans. Here, we describe the TOKs from four pathogens that cause the majority of life-threatening fungal infections in humans. These TOKs pass large currents only in the outward direction like the canonical isolate from *Saccharomyces cerevisiae* (ScTOK), and distinct from other K^+ channels. ScTOK, AfTOK1 (*Aspergillus fumigatus*), and H99TOK (*Cryptococcus neoformans grubii*) are K^+-selective and pass current above the K^+ reversal potential. CaTOK (*Candida albicans*) and CnTOK (*Cryptococcus neoformans neoformans*) pass both K^+ and Na^+ and conduct above a reversal potential reflecting the mixed permeability of their selectivity filter. Mutations in CaTOK and ScTOK at sites homologous to those that open the internal gates in classical K^+ channels are shown to produce inward TOK currents. A favored model for outward rectification is proposed whereby the reversal potential determines ion occupancy, and thus, conductivity, of the selectivity

Correspondence: Steve A. N. Goldstein, Departments of Physiology & Biophysics and Pediatrics, School of Medicine, Susan and Henry Samueli College of Health Sciences, University of California, Irvine, Irvine, CA 92697, USA. sgoldst2@uci.edu, Anthony Lewis, School of Pharmacy and Biomedical Sciences, Institute of Biological and Biomedical Sciences, University of Portsmouth, Portsmouth, Hampshire, PO1 2DT, UK. anthony.lewis@port.ac.uk.

AUTHOR CONTRIBUTIONS

A. Lewis and S.A.N. Goldstein designed the study and wrote the manuscript; A. Lewis cloned and characterized the wild type channels and analyzed data; A. Lewis, Z. McCrossan, and M. Popa performed mutagenesis experiments, characterized channels and analyzed data; R. Manville performed bioinformatics analyses. A. Lewis, S.A.N. Goldstein and L.G. Cuello devised the rectification model.

CONFLICT OF INTEREST

The authors declare no conflicts of interest.

filter gate that is coupled to an imperfectly restrictive internal gate, permitting the filter to sample ion concentrations on both sides of the membrane.

Keywords

Aspergillus; *Candida*; *Cryptococcus*; gating; potassium; selectivity

1 | INTRODUCTION

Potassium (K^+) channels are found across the kingdoms of life and are characterized by their structures and functions. Based on a predicted structure of two pore-forming domains in one subunit (2P), we identified genes encoding K^+ channel subunits with four transmembrane spans in animals (2P/4TM or K_{2P}) and a 2P/8TM subunit in *Saccharomyces cerevisiae*, ScTOK[1] (Figure 1A). Both K_{2P} and TOK channels showed operational attributes divergent from previously cloned K^+ channels that had subunits bearing 1P domain.[1–6]

We described ScTOK as an outward rectifier because it passes outward K^+ current at membrane potentials positive to the equilibrium reversal potential for K^+ (E_K) but little influx below E_K.[1] ScTOK has been correlated with the major outward K^+ current in yeast,[7] identified as a receptor for fungal killer toxin[8,9] and shown to regulate cellular membrane potential.[10] ScTOK homologues have been described in *Candida albicans*,[11] the root fungus *Neurospora crassa* (NcTOK)[12] and in the ectomycorrhizal fungus *Hebeloma cylindrosporum* (HcTOK2.2), the latter proposed to be important for symbiotic fungal-plant K^+ transfer.[13] Inward TOK channel currents have not been reported and the basis for outward rectification has remained unknown.[7,14–19]

Here, we compare TOKs cloned from four pathogenic fungi with ScTOK. Examination of open source genomic databases two decades after we identified ScTOK reveals that there are many TOK channels with 2P/8TM subunit topology in fungal genomes ([13,20] and this work) but none are apparent in other microorganisms, neither plants nor animals including humans. Seeking homologs for comparative studies, and appreciating that the most frequent life-threatening fungal infections are caused in patients with immunological impairment by the genera *Candida*, *Cryptococcus,* and *Aspergillus*,[21] we searched databases using ScTOK as bait, cloned and studied four 2P/8TM TOK homologues from the pathogens that operate as ion channels and a 2P/7TM subunit that does not. Comparison of the function of ScTOK and the new TOK channels, and variants with point mutations that permit inward currents, allow us to suggest a model for their distinctive function as outward rectifiers.

2 | MATERIALS AND METHODS

2.1 | Bioinformatics

Homologues of TOK were identified using BLASTP (protein-protein) searches against fungal databases compiled by the Joint Genome Institute (JGI) and the BROAD Institute using the putative sequence from *Saccharomyces cerevisiae* (CAA89386.1) as bait. Putative TOK sequences were verified using consensus prediction of membrane protein topology software (TOPCONS, topcons.cbr.su.se) to confirm predicted 8TM/2P structure and the

presence of two potassium selectivity filter sequences (TxGxGx). Alignment of identified TOK sequences was conducted using ClustalW 2.0 sequence alignment software (default settings, align order input, fast alignment). Phylogenetic analysis was conducted using the multiple alignment software MUSCLE v3.7 (default settings). Outputs were processed using GBLOCKS (default settings) to eliminate poorly aligned positions and divergent regions. Phylogenetic trees were constructed using PhyML v3.0 (bootstrapping at 100, substitution model WAG: protein) and the tree rendered using TreeDyn (www.phylogeny.fr/).

2.2 | Molecular biology

cDNA encoding partial 5′ and 3′ untranslated regions (UTR) and the longest open reading frame (ORF) of TOK homologues from *Aspergillus fumigatus* strain Af293 (Af), *Candida albicans* strain SC5314 (Ca) and two species of *Cryptococcus neoformans,* variations *neoformans* strain JEC21 (Cn) and *grubii* strain H99 (H99) were isolated by reverse transcription polymerase chain reaction (RT-PCR) from total RNA (*Aspergillus* and *Cryptococcus* total RNA were kind gifts from Dr David Askew, University of Cincinnati and Prof. Joseph Heitman, Duke University, respectively). RT-PCR was performed using IPROOF polymerase (Bio-Rad Laboratories, Hercules, CA) following the manufacturer's instructions, and using the following cloning primers; AfTOK1 forward, 5′-ATGGCGCCGCAAATAAAACACAAATCC-3′, AfTOK1 reverse, 5′-CATCGTTCAGTACATGAAGAAT CAC-3′; AfTOK-2 forward, 5′-AGGCCATGCGGTACGCAATGTTGC-3′, AfTOK-2 reverse, 5′-GGTTGGATGTGTCAAGACACCTAAT-3′, CaTOK forward, 5′-CTACCGAGTCTACAGTTGATCTTGGC-3′, CaTOK reverse, 5′-ACTACAGCTCCAATGGTCACCACATC-3′; CnTOK forward, 5′-ACCATCTCTATGCTCCAGCTAATGT-3′, CnTOK reverse, 5′-CATATGCCTGATGAAGATACCC TCT-3′; H99TOK forward, 5′-AGCTAATGTCTAGTCGCC-3′, H99TOK reverse, 5′-CGACAATGTTGGGTTTCATCAGAG-3′. An in-frame stop codon preceding an ATG start codon was used to determine the longest ORF for each gene product. PCR products were cloned into pCR2.1-TOPO (Invitrogen, Carlsbad, CA) and sequenced. Several independent reactions for each gene product were sequenced to account for any errors generated during PCR. Fully sequenced genes were submitted to NCBI with the following accession numbers: AfTOK1 (EU490498), AfTOK2 (EU490499), CaTOK (EU490500), CnTOK (EU490501), and H99TOK (EU490502). A second set of primers with flanking restriction sites were used to sub-clone the coding sequence (minus untranslated cDNA sequence) from the original pCR2.1-TOPO into pMAX, a modified pCR3.1 dual expression vector (Invitrogen, Carlsbad, CA) containing a T7 promoter for cRNA synthesis. Plasmid DNA was isolated using the Qiagen Miniprep Kit (Qiagen, Valencia, CA), linearized, and then purified using a Qiaquick PCR Purification Kit (Qiagen, Valencia, CA). cRNA was synthesized in-vitro using the T7 mMESSAGE mMACHINE kit (Ambion, Inc, Austin, TX). cRNA concentration and purity was determined by spectrophotometry and visualized for qualitative analysis by gel electrophoresis.

2.3 | Expression in Xenopus laevis oocytes

Xenopus laevis oocytes were prepared and isolated as before.[22] Briefly, frogs were anesthetized by an institution-approved protocol using a 1% tricaine solution (containing 5 mM HEPES, pH 7.5) for 10 minutes and stage IV-V oocytes isolated and defolliculated in Ca^{2+}-free OR-2 solution (in mM: 82.5 NaCl, 2.5 KCl, 1 $MgCl_2$, 10 HEPES, pH 7.4 NaOH) using collagenase (~1 hours in 2 mg/mL collagenase type II; Worthington). Oocytes were injected with 0.2–5 ng cRNA (23nl) and incubated in ND-96 supplemented with 50 μg/mL gentamycin and 1% of penicillin/streptomycin at 16°C. ND-96 solution contained (in mM) 96 NaCl, 2 KCl, 1 $MgCl_2$, 1.8 $CaCl_2$, 10 HEPES (pH 7.6, NaOH). For studying potential AfTOK1 heteromer channels formed with AfTOK2 or AfTOK3, cRNA was injected at a 1:25 ratio (AfTOK1:AfTOK2 or AfTOK3).

2.4 | Electrophysiology

Whole-cell currents were measured 1–3 days post-injection using a Geneclamp 500 amplifier and Axon Digidata 1322 (Axon Instruments, Foster City, CA). Microelectrodes were filled with 3 M KCl and had tip resistances of 0.2–1.0 MΩ. Currents were recorded at room temperature with constant solution flow at 1–2 mL/min with bath solution containing (in mM): 96 NaCl, 4 KCl, 1 $MgCl_2$, 0.3 $CaCl_2$, 10 HEPES (pH 7.6, tris-base). Reagents were from Sigma unless stated otherwise. Stock solutions of tetraethylammonium (TEA), calcium chloride ($CaCl_2$), and barium chloride ($BaCl_2$) were dissolved in deionized water and diluted to the required concentrations in standard bath solution prior to experimentation. Data were sampled at 5 kHz, filtered at 1 kHz and recorded using Clampex 9.1 software (Axon Instruments, Inc). Currents were not adjusted for leak or capacitance. Oocyte membrane potential was held at −80 mV and step depolarized to potentials ranging from −120 mV to +60 mV in 10 mV steps for a duration of 1–3 seconds. This was followed by a second voltage step to −30 mV for 0.5–1 seconds to visualize tail currents before returning to the holding potential. For selectivity measurements, NaCl was isotonically substituted for KCl to give a final $[K^+]_o$ of 4, 20, and 100 mM. Liquid junction potentials were less than 4 mV and were not subtracted when generating current-voltage curves. For ionic substitution experiments, 100 mM K^+ was replaced with 100 mM of Rb^+, Na^+, Li^+, or Cs^+; under these conditions reversal potential measurements were adjusted for liquid junction potentials.

2.5 | Data analysis and statistics

Data were analyzed using Clampfit 9.1 (Axon Instruments, Inc), tabulated in Excel (Microsoft Office 2003) and plotted using Origin 6.1 software (Origin Lab, Northampton, MA). Current-voltage (I-V) relationships were generated from steady-state currents at potentials between −120 mV and 60 mV. Conductance values were obtained by dividing the peak current by the electrochemical driving force ($I_K/(V_m - E_k)$), where $[K^+]_i$ is 140 mM. Normalized conductance-voltage relationships were obtained by normalizing conductance (G) to maximal conductance (G_{max}) at +60 mV and fitted using the Boltzmann equation ($G = G_{max}/[1 + \exp(V - V_{0.5}/k)]$, where $V_{0.5}$ is the half-maximal activation and k is the slope factor.

3 | RESULTS

3.1 | Genomic analysis and cloning of TOK channel genes from four fungal species

Searching the subset of fungal databases with the ScTOK protein sequence as bait identified 205 TOK-like channel homologues in 25 human pathogens, 11 animal pathogens, 34 phytopathogens, and 135 described as non-pathogenic fungi. Some fungal genomes revealed a single TOK-related gene whereas others, such as *Aspergillus* species *niger*, *fumigatus, terreus and fischeri* (also known as *Neosartorya fischeri*), have multiple homologous genes. When the sequences for the 25 predicted TOK-like proteins from human pathogenic species identified in the NCBI database were compared (Figure 1), the channels fell into three distinct groups by species, *Aspergillus*, *Candida,* and *Cryptococcus*, and a multispecies clade that included pathogens that are all associated with skin lesions.[21,23,24]

Here, the four pathogens that cause the majority of fatal infections in immunocompromised humans[21] are studied in greater depth: two ascomycetes, *Aspergillus fumigatus* and *Candida albicans*, and two basidiomycetes, *Cryptococcus neoformans* variants *neoformans* and *grubii*. Among the four pathogens, only *Aspergillus fumigatus* has more than one predicted TOK-like locus, carrying three, one each on chromosomes 1, 3, and 8. Four genes encoding 2P/8TM proteins and one predicting a 2P/7TM subunit were cloned. The cloning of the *Candida albicans* TOK gene by others has been described previously.[11]

To isolate full-length cDNAs for the TOK-like genes, RT-PCR was performed using DNaseI-treated total RNA from each of the four fungal species. In-frame stop codons upstream of an ATG start codon were used to determine the longest open reading frame for the four 2P/8TM subunits: *Aspergillus fumigatus* TOK1 (AfTOK1, 699 aa), *Candida albicans* TOK (CaTOK, 741 aa), *Cryptococcus neoformans* (CnTOK, 807 aa), and *Cryptococcus grubii* (H99TOK, 821 aa); these sequences predict molecular masses of ~79, ~84, ~91, and ~92 kD, respectively. Hydropathy analysis predicted these subunits to have topologies like ScTOK with intracellular N- and C-termini, eight TM segments, and P domains between TM5-TM6 and TM7-TM8 bearing classical K^+-selectivity signature sequences (Figure 2). Inter-species homology was low, showing ~24%−37% of amino acid identity primarily in the P domains and their flanking TM spans, whereas the two *Cryptococcal* isolates were 86% identical. No TM span was predicted to carry more than two charged residues suggesting the absence of a voltage sensor domain like that found in voltage-gated K^+ (K_V) channels.

While cloning confirmed the TOK gene on *Aspergillus fumigatus* chromosome 1 to predict a 2P/8TM protein (AfTOK1), the TOK-like sequence on chromosome 3 appeared to be a 2P/8TM gene punctuated by stop codons, inconsistent with coding of either a 1P or 2P K^+ channel subunit because the longest ORF encoded a 48-residue peptide (AfTOK3). The TOK-like gene on chromosome 8 predicted a 2P/7TM protein of 593 residues that appeared to lack TM1 (AfTOK2). This was consistent with prior database analyses by others describing genes for four proteins with 2P/7TM topology including AfTOK2, NfTOK2 in *Neosartorya fischeri*, AnTOK2 in *Aspergillus niger* and AtTOK2 in *Aspergillus terreus*[15] that cluster in a phylogenic tree (Figure 1).

3.2 | Newly cloned TOKs are outward rectifiers like ScTOK with functional variations

The electrophysiology of ScTOK and the new homologs was assessed by heterologous expression in *Xenopus laevis* oocytes using two-electrode voltage clamp. ScTOK is K^+-selective outward rectifier[1]; that is, it passes K^+ ions outward and is active only above a threshold voltage that varies with the transmembrane concentration gradient of K^+ that establishes the equilibrium reversal potential for K^+, E_K (Figure 3A,B, and Table 1). As before, ScTOK was found to be selective for K^+ over Na^+ ($P_{Na}/P_K = 0.04$, Table 2). A 10-fold change in external KCl shifted the reversal potential by 50 mV (Figure 3C and Table 1) similar to the value of 58.2 mV for an ideal K^+-selective pore under these conditions. Other distinctive features of ScTOK included activation upon depolarization that showed two components, one that was rapid and contributed ~80% of total current by 1 second with 4 mM KCl in the bath, and a slow phase (Figure 3A and Table 1). Also characteristic of ScTOK was deactivation upon repolarization that was too rapid to differentiate from the capacitive transient and the absence of apparent inactivation during depolarizing pulses.

Like ScTOK, the four 2P/8TM subunits AfTOK1, CaTOK, CnTOK, and H99TOK produced robust outward K^+ currents that were not observed with control oocytes (Figure 3A). Since the 2P domains in TOK channels are located between TM5-TM6 and TM7-TM8 (Figure 2A) and are expected to form a single central conduction pathway via dimerization as seen with 2P/4TM channels,[25,26] it was reasonable to assume the 2P/7TM subunit AfTOK2 lacking TM1 might pass current on its own, or modify the operation of AfTOK1. However, neither new currents were seen in oocytes injected with cRNA for AfTOK2, or the small peptide AfTOK3, nor did either modify operation of the 2P/8TM subunit AfTOK1 on co-expression. AfTOK2 and AfTOK3 were not studied further.

3.2.1 | Activation threshold for outward current varies with ionic selectivity—

Like ScTOK, AfTOK1, and H99TOK pass outward currents above E_K, whereas CnTOK and CaTOK showed a threshold potential for activation that was more depolarized (Table 1). Consistent with the notion that the threshold for outward current varied as a function of channel discrimination among permeant monovalent cations, CnTOK and CaTOK were less selective for K^+ over Na^+ compared to ScTOK, AfTOK1, and H99TOK (Figure 3C and Table 1). Indeed, the threshold potential for all the TOKs was well approximated using their determined relative permeability for K^+ and Na^+ and the values of E_K and E_{Na} at bath KCl concentrations of 4 mM, 20 mM, and 100 mM using the Goldman-Hodgkin-Katz (GHK) current equation (Table 1).

Changes in bath KCl shifted not only the activation threshold, but also steady-state current magnitude (Figure 3B). Increasing bath KCl from 4 to 100 mM reduced the magnitude of steady-state currents in all TOK channels, having the greatest effect on CaTOK (~90%). However, the reduction did not correlate with the theoretical reduction in current predicted by the Goldman-Hodgkin-Katz (GHK) flux equation for a K^+-selective pore, consistent with permeation by Na^+. CaTOK and CnTOK also showed greater relative permeability for Na^+ than AfTOK1, H99TOK, and ScTOK, as determined by studying reversal potentials after isotonic substitution of 100 mM bath KCl with NaCl (Table 2). Similarly, the alkali metals

Rb^+ and Cs^+ had greater relative permeability in CaTOK than other TOK channels whereas Li^+ had a greatest relative permeability in CnTOK.

3.2.2 | Rapid and slow phases of activation correlate with K^+-selectivity—

Despite the absence of classical voltage-sensing residues, normalized conductance-voltage relationships revealed differences among the channels in the voltage-dependence of steady-state channel activation. Half-maximal activation potentials ($V_{½}$) varied from −50 mV for AfTOK1 to +14 mV for CnTOK with 4 mM extracellular KCl (Table 1). We were unable to assess G/V relationships for higher levels of bath KCl because the conductance failed to saturate even at +200 mV and the absence of detectable deactivation kinetics for ScTOK and AfTOK1 precluded comparison of tail currents.

Like ScTOK, AfTOK1, and H99TOK currents showed a prominent immediate rise in the current with voltage steps and the fraction of current that developed rapidly decreased as bath KCl increased (Table 1). In contrast, the less selective channels CaTOK and CnTOK showed no immediate activation, developing current in response to voltage steps in a fully time-dependent manner. Furthermore, time-dependent currents for H99TOK, CnTOK, CaTOK, and ScTOK were slowed by increasing bath KCl and found to be faster to develop and more sensitive to elevation of bath KCl in the order of their selectivity for K^+ (H99TOK > CnTOK>CaTOK).

Like ScTOK, AfTOK1 currents decayed too rapidly on repolarization to quantify (Figure 3 and Table 1). In contrast, H99TOK, CnTOK, and CaTOK exhibited time-dependent deactivating tail currents to −30 mV, well fit by a single exponential; these decay rates were notable for correlating with selectivity, those channels displaying Na^+ permeability taking longer to close. All the new TOKs, like ScTOK, showed no inactivation of currents during depolarizing steps lasting 1 second.

3.3 | Unlike ScTOK, wild-type H99TOK passes small inward currents

ScTOK did not pass inward K^+ currents despite driving forces that strongly favored influx; thus, no inward currents were observed at −120 mV with levels of bath KCl of 4 mM (E_K ~ −90 mV, Figure 3A), 100 mM (E_K ~ −9 mV, Figure 3B), or 300 mM (E_K ~ +19 mV, n = 5) even after 1 second depolarizing pulses to open the channels. Arguing against a blocking mechanism for outward rectification, ScTOK showed no inward currents on removal of Mg^{2+}, Ca^{2+}, or Na^+ from the bath solutions even when ultrapure KCl was employed to diminish trace heavy metals present in standard grade reagents. Similarly, no inward currents were observed with AfTOK1, CaTOK, or CnTOK at −120 mV with 4 mM KCl or 100 mM KCl in the bath. In contrast, H99TOK showed small inward currents at potentials below E_K with 100 mM bath KCl (Figure 3B, inset). This suggested that TOK channels might not achieve outward rectification via a novel mechanism but rather employ a variation of known K^+ channel gating mechanisms. Evidence for classical gating mechanisms was sought.

3.4 | Scanning mutagenesis of CaTOK identifies “gating hinge” sites that allow inward current

Transmembrane spans that follow the single P loop present in K^+ channels of known 3D structure form inner pore-lining helices that bend at a glycine “gating hinge” to produce a “bundle crossing” constriction in the closed state.[27] Moreover, mutations in this hinge region can favor the open conformation.[28,29] Therefore, we evaluated the S6 and S8 domains of CaTOK by serial point mutation of each residue to Asp, Asn, or Ala. The mutational scans of CaTOK revealed three positions in the S6 span (G337, V338, and G342) where mutations produced inward currents. No similar sites were found in the S8 span (Figure 4). CaTOK position G342 was studied in detail.

The G342D mutation in CaTOK channels that permitted passage of inward K^+ current, speeded channel activation and deactivation, and increased selectivity for K^+ over Na^+ (Figure 5A,C). Thus, current activation was largely instantaneous and deactivation at −30 mV was too rapid to separate from the capacitive transient. The activation threshold and $V_{½}$ were left-shifted by ~24 mV and ~40 mV, respectively, consistent with increased selectivity for K^+ over Na^+ (Table 3 and Figure 5B,C).

Increasing extracellular KCl from 4 mM to 100 mM increased inward currents below E_K through CaTOK-G342D channels. The inward current magnitude was not linear with voltage, reaching a maximum before declining with further hyperpolarization (Figure 5D). Reversal potential plotted as a function of varying bath KCl from 4 and 100 mM confirmed that the mutation increased K^+ ion selectivity over Na^+ showing a change in reversal of 52 ± 1.0 mV with a 10-fold change in bath KCl compare to 28 ± 1.0 mV for the wild type channel (Figure 5C). Isotonic replacement of external KCl with RbCl increased the magnitude of inward current and attenuated the decline in current with hyperpolarization (Figure 5D).

Substitution with Asn (CaTOK-G342N) produced a channel with similar attributes as CaTOK-G342D indicating that the change in selectivity and passage of inward currents did not require the acidic residue. In contrast, substitution with Ala, Phe, Glu, Ser, Cys, Leu, and Gln generated channels that showed no inward currents, albeit with variations in other gating parameters, and CaTOK-G342K channels passed no current (Table 3). Moreover, mutation of CaTOK residue G342 to N produced channels that were less sensitive to Ba^{2+} blockade (Figure 5E, IC_{50} WT, 54.2 ± 8.9 μM versus G342N 8.3 ± 0.9 mM). CaTOK-V338D channels showed characteristics like those observed with CaTOK-G342D (Figure 6).

3.5 | Analogous mutations at the ScTOK gating hinge residues allow inward currents

To determine if the effects of the mutations in CaTOK were serendipitous, the same positions were altered in ScTOK. Supporting the notion that the observations identify residues key to outward rectification, inward K^+ and Rb^+ currents were observed when two equivalent positions in ScTOK, V312, and G316, were mutated to Asp and Asn but not Ala (Figures 6 and 7). In contrast, ScTOK-G311D (equivalent to CaTOK-G337D) did not produce inward currents.

3.6 | Permeant ions dictate gating kinetics

Comparison of the biophysical properties of CaTOK channels harboring different amino acids at position G342 revealed a correlation between gating parameters and relative permeant ion species (Table 3). Mutations that generated channels with higher relative selectivity for K^+ over Na^+ (Asp, Glu, Asn, Gln), as judged by their reversal potential with different bath KCl levels, showed more negative thresholds for activation and hyperpolarized $V_{½}$ compared to wild type channels and largely instantaneous currents with little or no deactivating tail currents. In contrast, mutations with lower relative selectivity (Cys, Phe, Leu) showed more positive thresholds for activation and $V_{½}$ (similar to wild type) and activated in a time-dependent manner, displaying little, or no instantaneous kinetics. Mutations with ion selectivity intermediate of these two defined groups (Ala, Ser) showed transitional gating properties.

4 | DISCUSSION

In this report, we highlight the distribution of TOK channels across fungal phyla and study examples from four species of human pathogenic fungi. One motivation for this study of fungal K_{2P} (TOK) channels is that their expression in fungi but not humans, unique structure and function, and the lethal effects of excess TOK activity in yeast,[8,9] all suggest that TOK channels have potential as targets for anti-mycotic therapy. Another goal of the investigation was to explore the unusual outward rectification of the canonical isolate ScTOK.[1] The biophysical attributes of the four newly cloned channels suggest that all TOK channels will operate as outward rectifiers. Thus, large outward currents are observed above E_K for the K^+- selective TOK channels and above a reversal potential determined by the mixed ionic selectivity for channels that pass other monovalent cations as well. Thus, ScTOK, AfTOK1, CaTOK, and CnTOK do not pass inward currents in wild type form even though CaTOK and CnTOK conduct Na^+. In contrast, H99TOK channels show small inward currents suggesting the restriction to inward flux is not absolute and altering single residues in ScTOK and CaTOK at sites homologous to those that form an inner gating hinge in 1P K^+ channels were found to permit inward currents. Further, the ion selectivity of TOK channels appears to dictate not only their voltage-threshold for activation, but also gating kinetics, a conclusion supported by scanning mutations in CaTOK. The findings lead us to suggest that gating structures and mechanisms in 1P domain K^+ channels are sufficient to explain the unidirectional outward ion flux observed in TOK channels. We interpret the data to be most consistent with the idea that TOK channels have a filter gate and a leaky bundle-crossing inner gate similar to that in 1P domain K^+ channels (or that the bundle restriction is thwarted by fenestration) so the selectivity filter can sample ion concentrations on opposite sides of the membrane.

4.1 | An updated state model for TOK gating

ScTOK shows two activation components, one slow and the other fast, and a single, very rapid deactivation transition. Historically, this has been attributed to two gates; one residing at the selectivity filter and another at an internal position reminiscent of the helix bundle crossing of 1P voltage-gated K^+ channels (K_V) creating a three state model $C_X \leftrightarrow R \leftrightarrow O$,[4] where C_X comprises a set of related, slowly activating states attributed to the movement of a

restrictive inner gate, R represents a non-conductive state ascribed to the filter that activates very rapidly, and O is the open state. The extremely rapid closure of the channel (deactivation) is attributed to the reverse of the rapid R ↔ O transition. In support of this idea, Loukin and coworkers model ScTOK with two closed states with distinct temperature dependence (ΔT), a slow transition with ΔT typical of protein conformational changes (C ↔ R) that they posit to be the movement of an internal gate, and another closed state from which opening is extremely rapid with a ΔT like ionic diffusion (R ↔ O) that they attribute to the filter.[18] Although AfTOK1 opens nearly instantaneously and CaTOK activation is fully time-dependent (Figure 3A and Table 1), both can be accommodated by these three state models. In contrast, H99TOK, CnTOK, and CaTOK exhibit time-dependent deactivating tail currents to membrane voltages above E_K (with single exponential decay rates notable for correlating with their ion selectivity) and instantaneous closure to voltages below E_K and this suggests that TOK channel gating models require at least two ways to close, such as, $C_X \leftrightarrow O_X$ and $R \leftrightarrow O_X$, rather than a linear three state model (Figure 8B).

4.2 | An ion occupancy model for outward rectification and TOK gating kinetics

The ion conduction pathway in K^+ channels formed by four 1P subunits opens and closes at two gates, an inner helix bundle gate that restricts access of hydrated cytoplasmic K^+ ions to the selectivity filter gate in closed channels. The inner gate in 1P channels is coupled to the filter gate such that depolarization re-orientates the inner helices around a hinge to open the conduction pathway and this promotes subsequent closing of the filter in a process called inactivation.[30] In contrast, neither structural nor functional data support the presence of a restrictive physical inner gate in the 2P/4TM (K_{2P}) channels.[31–38] Lack of restriction at the lower gate, however, does not preclude maintenance of coupling of the inner “gate” region and the pore filter, as we have demonstrated.[38] This idea is consistent with observation in molecular dynamics simulations that small changes at the internal gate in KcsA can allow rapid pore-filter opening from a closed, pre-conductive state[39] that is primed for permeation,[40] and electrophysiology studies on voltage-gated K^+ channels that argue a final gating step follows movement of all four voltage-sensors into a permissive conformation.[41]

Both 1P and 2P/4TM (K_{2P}) channels of known structure have ion selectivity filters with at least six ion binding sites (Figure 8A); one on the outside face of the selectivity filter (S0), four in the filter (S1-S4) and a site within the internal cavity below the filter (S5). Two models for ion occupancy of these sites have been proposed to explain pore-filter control of permeation and inactivation. In the “canonical” model that we favor, ion occupancy in the pore alternates between two iso-energetic configurations where S1/S3 sites are occupied by K^+ ions (with S2/S4 sites occupied by water), or with K^+ ions in the S2/S4 sites[42,43]; this model is supported by structural studies,[43–47] molecular dynamics simulations,[48] and streaming potential measurements,[49–51] across multiple potassium channel subtypes.[42] In the “hard knock-on” model, all four sites in the pore are occupied simultaneously (no water molecules interposed), permeation occurs through direct Coulomb repulsion between adjacent ions,[52] and sub-optimal ion occupancy in the pore-filter (<4) is predicted to disrupt ion selectivity and induce pore inactivation. Arguing against this model, a recently published structure of KcsA with a T75A mutation that disrupts the S4 binding site, preventing all four sites from being occupied simultaneously, was demonstrated to be K^+-selective and non-

inactivating and the homologous change in two voltage-gated potassium channels retained selectivity while suppressing C-type inactivation.[46]

Thus, we rationalize TOK operation via the canonical model, as follows. Inward driving force favors K^+ in the S1 TOK site, and thus, decreased occupancy of S2 (Figure 8A), a state that has been associated in KcsA with an over 10-fold decrease in unitary conductance,[53] and over a 10-fold decrease in open probability,[54] effects that would yield negligible inward current rapidly. This is also consistent with free energy perturbation molecular dynamics that show the absence of ion in S2 favors pore filter collapse.[55] Conversely, when driving force is outward (above E_K), we propose that the S4 site is occupied favoring a 2/4 ion profile favoring a conductive state of the filter.

Our TOK model bears similarities to the intra-filter gating mechanism suggested by Loukin and Saimi,[18] and provides a subtle mechanism coupling a leaky inner gate region and the selectivity filter gate. We speculate that mutations at the inner gate region (in CaTOK at 338 and 342 or in ScTOK at 312 and 316) favor the conductive filter conformation regardless of the direction of ion flow. The effects of the mutations we describe are consistent with studies of K_{2P} channels at the site equivalent to CaTOK-342 and ScTOK-316 that altered open probability and gating kinetics.[29,56] Studies of voltage-gated (1P) K^+ channels also align with this model; molecular dynamics simulations of Shaker-A471D (a site homologous to CaTOK-342 and ScTOK-G316), where replacement of the natural hydrophobic residue with a hydrophilic residue increased K^+ occupancy of the inner channel vestibule.[57] The observation that mutations inducing inward currents were only identified in S6 and not S8, likely reflects the asymmetry of the transmembrane domains that line the inner cavity of K_{2P} channels[25,32] and the evolutionary conservation of residues in S6 across TOK sequences,[58] suggestive of a prominent role in dictating gating and permeation characteristics.

Mutation of the S4 site in K_{2P} channels has been shown to generate channels with instantaneous kinetics and linear IV relationships.[59] Here, we propose that mutations to the inner vestibule enhance K^+ ion binding at S4, promoting open rectification. Consistent with this notion, Ba^{2+} and K^+ ions compete for binding at the S4 site in K_{2P} channels,[60] and CaTOK-G342N shows decreased Ba^{2+} sensitivity that may reflect stabilization of K^+ ion in the S4 site by the inner vestibule mutation. Furthermore, a critical role for the S4 site has been previously highlighted in the allosteric coupling between the inner gate and the selectivity gate the 1P K^+ channels KcsA, Kv1.5 and *Shaker*.[61]

Our model justifies the reduced magnitude of inward currents observed in the CaTOK and ScTOK inner gate mutants as membrane potential becomes increasingly negative (Figures 5D, 6B, and 7B) as follows; at more hyperpolarized voltages, occupancy of outer pore sites would be expected to increase, relative to the inner vestibule promoting a 1/3 ion profile and a non-conductive filter. CaTOK and ScTOK pore mutants show an increase in inward current when external RbCl replaces KCl, in line with previous observations that Rb^+ decreases the rate of pore-mediated C-type inactivation in KcsA,[62] *Shaker*[63] and Ca^{2+}-activated K^+ channels[64] and induces stabilization of the open state of the selectivity filter gate in K_{2P} channels.[56] Furthermore, macromolecular crystallization studies of KcsA

support the idea that Rb^+ ions stabilize its conductive conformation because the ions halt structural changes of the filter associated with C-type inactivation gating.[62]

TOK channels display a decrease in outward current at high external K^+, beyond what can be explained by changes in driving force (Figure 3B). In our model, when external K^+ is increased but driving force is still directed outward (above E_K), inner pore sites would be occupied by outward ion flux favoring a 2/4 ion filter profile and conduction. Countering this effect, high external K^+ would increase residency of the outer pore sites promoting an S1/S3 ion profile and the non-conductive state. Thus, we hypothesize it is the balance of K^+ occupancy at the inner and outer pore sites that leads to a greater than Nernstian decrease in outward current with high bath K^+. We propose this effect of high external K^+ was mitigated in the CaTOK-G342D and ScTOK-G316D channels (Figures 5 and 7) due to favorable occupancy of inner sites in the mutants compared to the wild type channels. The need for caution is made apparent by studies that conclude occupancy of S2 in KcsA favors pore-mediated inactivation,[53,65,66] however, those studies employ closed-channel structures in contrast to those used to devise our model[54,55] where the activation gate is open, the state that allows pore-filter inactivation.

4.3 | Ion selectivity, allosteric coupling, and gating kinetics in TOK channels

Our data show that ion selectivity correlates with activation kinetics such that channels that are more selective for K^+ have phases of near-instantaneous activation that are prominent (AfTOK1 and ScTOK) while those that are Na^+ permeable (CaTOK and CnTOK) activate in a fully time-dependent manner. We propose time-dependent activation in TOK channels that pass Na^+ may be explained by an effect by inner pore ion occupancy on the non-restrictive inner gate and coupling to the selectivity filter gate (Figure 8). Coupling is well established in 1P channels where opening of the lower gate influences the state and selectivity of the filter gate.[30,67] Further, mutations in the selectivity filter of the NaK channels produce rearrangements at the inner gate[68] and a filter mutation in KcsA inverts allosteric coupling so that activation of the inner gate favors a conductive pore rather than inactivation.[61] We demonstrated coupling as well in 2P channels that lack a restrictive internal gate, showing that intracellular phosphorylation-induced closure of the K_{2P} channel KCNK0 could not proceed until barium exited the channel pore filter.[38] Further, intracellular Na^+ alters slow gating transitions to decrease in open probability of KcsA,[69] Na^+ ions can occupy the S5 site,[70,71] and mutations that change electrostatics in the inner cavity can alter selectivity of this site for K^+ over Na^+.[72] Thus, we propose that internal Na^+ rather than K^+ yields time-dependent structural rearrangements of the non-restrictive inner gate and that mutations of S6 TM residues in CaTOK that improve K^+ selectivity thereby remove time dependent activation (Table 3).

4.4 | Comparison with other proposed K_{2P} channel gating models

4.4.1 | C-type (pore) inactivation—

K_{2P} and 1P K^+ channels both utilize the filter gate to control ion conduction. Whereas 1P channels have a restrictive lower gate, 2P/4TM channels show restrictive gating exclusively at the selectivity filter[38] and thereafter.[31–37] A non-restrictive internal gate is also described for CNG channels.[73] Here, we suggest that TOK channels employ a similar type of filter gate control (based on ion residency at the S2

site), however, the mechanisms cannot be identical because increased external K^+ reduces TOK channel activity (Loukin and Saimi18 and this work; Figure 3A and Table 1) whereas it slows channel inactivation (and closure) in K_{2P} and 1P K^+ channels.

4.4.2 | Ion-flux gating—Schewe and colleagues propose a gating model for mammalian K_{2P} channels,[59] whereby the filter is either depleted or fully occupied by ions as a function of the equilibrium potential, and then, reverts to 1/3 or 2/4 ion occupancy. This model posits that the filter only fills with ions from the cytosol with outward driving force and cannot serve to explain TOK operation where both the non-conductive (R) state can sample K^+ from both the inner and outer solutions, a case made cogently by Loukin and Saimi.[18]

4.4.3 | Hydrophobic gating model—K_{2P} and 1P BK channels are proposed to lack a physically restrictive internal gate and changes in pore geometry and hydrophobicity are suggested to generate free energy barriers to ion permeation via “hydrophobic dewetting transitions” that are disrupted by introduction of hydrophilic residues in the cavity.[74,75] In the case of the BK channel, molecular dynamic simulations reveal that replacing an alanine with aspartate at position homologous to the CaTOK-G342 and ScTOK-G316 leads to a fully solvated pore, allowing ions to access the selectivity filter readily.[75] As this position (and mutation) are homologous to the CaTOK-G342D and ScTOK-G316D mutations that generate inward current in TOK channels, the hydrophobic gating proposal could prove applicable to operation of TOK channels.

ACKNOWLEDGMENTS

This research was funded by the Biotechnology and Biological Sciences Research Council (BBSRC), UK, Grant Number BB/J006114/1 to A. Lewis., NIH RO1GM097159 to L.G. Cuello and NIH RO1NINDS058505 to SAN Goldstein.

Funding information

HHS | NIH | National Institute of Neurological Disorders and Stroke (NINDS), Grant/Award Number: RO1NS58505; HHS | NIH | National Heart, Lung, and Blood Institute (NHLBI), Grant/Award Number: RO1HL61657; Biotechnology and Biological Sciences Research Council, Grant/Award Number: BB/J006114/1; HHS NIH National Institute of General Medical Sciences (NIGMS), Grant/Award Number: RO1GM097159

Abbreviations:

1P	single pore domain
2P	two-pore domain
Af	Aspergillus fumigatus
Ca	Candida albicans
Cn	Cryptococcus neoformans
E_K	equilibrium potential for potassium ions
E_{REV}	reversal potential
GHK	Goldman-Hodgkin-Katz

IC_{50}	half-maximal effective inhibitory concentration
K_V	voltage-gated potassium (channel)
K_{2P}	two-pore potassium (channel)
Sc	Saccharomyces cerevisiae
TEVC	two-electrode voltage clamp
TM	transmembrane (domain)
TOK	two-pore outwardly rectifying potassium (channel)
V½	half-maximal activation voltage

REFERENCES

1. Ketchum KA, Joiner WJ, Sellers AJ, Kaczmarek LK, Goldstein SAN. A new family of outwardly-rectifying potassium channel proteins with two pore domains in tandem. Nature. 1995;376:690–695. [PubMed: 7651518]
2. Goldstein SAN, Price LA, Rosenthal DN, Pausch MH. ORK1, a potassium-selective leak channel with two pore domains cloned from *Drosophila melanogaster* by expression in *Saccharomyces cerevisiae*. Proc Natl Acad Sci. 1996;93:13256–13261. [PubMed: 8917578]
3. Lesage F, Guillemare E, Fink M, et al. TWIK-1, a ubiquitous human weakly inward rectifying K+ channel with a novel structure. EMBO J. 1996;15:1004–1011. [PubMed: 8605869]
4. Lesage F, Guillemare E, Fink M, et al. A pH-sensitive yeast outward rectifier K+ channel with two pore domains and novel gating properties. J Biol Chem. 1996;271:4183–4187. [PubMed: 8626760]
5. Goldstein SAN, Wang KW, Ilan N, Pausch M. Sequence and function of the two P domain potassium channels: implications of an emerging superfamily. J Mol Med. 1998;76(1):13–20. [PubMed: 9462864]
6. Sesti F, Shih T, Nikoleva N, Goldstein SAN. The basis for immunity to killer toxin: channel block. Biophys J. 2001;80:446a.
7. Bertl A, Bihler H, Reid JD, Kettner C, Slayman CL. Physiological characterization of the yeast plasma membrane outward rectifying K+ channel, DUK1 (TOK1), in situ. J Membr Biol. 1998;162:67–80. [PubMed: 9516239]
8. Ahmed A, Sesti F, Ilan N, Shih TM, Sturley SL, Goldstein SAN. A molecular target for viral killer toxin: TOK1 potassium channels. Cell. 1999;99:283–291. [PubMed: 10555144]
9. Sesti F, Shih TM, Nikolaeva N, Goldstein SA. Immunity to K1 killer toxin: internal TOK1 blockade. Cell. 2001;105:637–644. [PubMed: 11389833]
10. Maresova L, Urbankova E, Gaskova D, Sychrova H. Measurements of plasma membrane potential changes in *Saccharomyces cerevisiae* cells reveal the importance of the Tok1 channel in membrane potential maintenance. FEMS Yeast Res. 2006;6:1039–1046. [PubMed: 17042753]
11. Baev D, Rivetta A, Li XS, et al. Killing of Candida albicans by human salivary histatin 5 is modulated, but not determined, by the potassium channel TOK1. Infect Immun. 2003;71:3251–3260. [PubMed: 12761106]
12. Roberts SK. TOK homologue in *Neurospora crassa*: first cloning and functional characterization of an ion channel in a filamentous fungus. Eukaryot Cell. 2003;2:181–190. [PubMed: 12582135]
13. Guerrero-Galan C, Delteil A, Garcia K, et al. Plant potassium nutrition in ectomycorrhizal symbiosis: properties and roles of the three fungal TOK potassium channels in *Hebeloma cylindrosporum*. Environ Microbiol. 2018;20:1873–1887. [PubMed: 29614209]
14. Roller A, Natura G, Bihler H, Slayman C, Eing C, Bertl A. In the yeast potassium channel, Tok1p, the external ring of aspartate residues modulates both gating and conductance. Pflügers Archiv Eur J Physiol. 2005;451:362–370. [PubMed: 16133265]

15. Roller A, Natura G, Bihler H, Slayman C, Bertl A. Functional consequences of leucine and tyrosine mutations in the dual pore motifs of the yeast K+ channel, Tok1p. Pflügers Archiv Euro J Physiol. 2008;456:883–896. [PubMed: 18421473]
16. Zhou XL, Vaillant B, Loukin SH, Kung C, Saimi Y. YKC1 encodes the depolarization-activated K + channel in the plasma membrane of yeast. FEBS Lett. 1995;373:170–176. [PubMed: 7589459]
17. Loukin SH, Vaillant B, Zhou XL, Spalding EP, Kung C, Saimi Y. Random mutagenesis reveals a region important for gating of the yeast K+ channel Ykc1. EMBO J. 1997;16:4817–4825. [PubMed: 9305624]
18. Loukin SH, Saimi Y. K+-dependent composite gating of the yeast K+ channel, Tok1. Biophys J. 1999;77:3060–3070. [PubMed: 10585928]
19. Loukin SH, Lin J, Athar U, Palmer C, Saimi Y. The carboxyl tail forms a discrete functional domain that blocks closure of the yeast K+ channel. Proc Natl Acad Sci. 2002;99:1926–1930. [PubMed: 11854493]
20. Prole DL, Taylor CW. Identification and analysis of cation channel homologues in human pathogenic fungi. PLoS One. 2012;7:e42404. [PubMed: 22876320]
21. Brown GD, Denning DW, Gow NA, Levitz SM, Netea MG, White TC. Hidden killers: human fungal infections. Sci Transl Med. 2012;4:165rv113.
22. Rajan S, Plant LD, Rabin ML, Butler MH, Goldstein SAN. Sumoylation silences the plasma membrane leak K^+ channel K2P1. Cell. 2005;121:37–47. [PubMed: 15820677]
23. Squeo RF, Beer R, Silvers D, Weitzman I, Grossman M. Invasive *Trichophyton rubrum* resembling blastomycosis infection in the immunocompromised host. J Am Acad Dermatol. 1998;39:379–380. [PubMed: 9703159]
24. Shiraki Y, Ishibashi Y, Hiruma M, Nishikawa A, Ikeda S. Cytokine secretion profiles of human keratinocytes during *Trichophyton tonsurans* and Arthroderma benhamiae infections. J Med Microbiol. 2006;55:1175–1185. [PubMed: 16914646]
25. Kollewe A, Lau AY, Sullivan A, Roux B, Goldstein SAN. A structural model for K2P potassium channels based on 23 pairs of interacting sites and continuum electrostatics. J Gen Physiol. 2009;134:53–68. [PubMed: 19564427]
26. Brohawn SG, del Marmol J, MacKinnon R. Crystal structure of the human K2P TRAAK, a lipid- and mechano-sensitive K+ ion channel. Science. 2012;335:436–441. [PubMed: 22282805]
27. Jiang Y, Lee A, Chen J, Cadene M, Chait BT, MacKinnon R. The open pore conformation of potassium channels. Nature. 2002;417:523–526. [PubMed: 12037560]
28. Brown S, Sonntag DP, Sanguinetti MC. A highly conserved alanine in the S6 domain of the hERG1 K+ channel is required for normal gating. Cell Physiol Biochem. 2008;22:601–610. [PubMed: 19088442]
29. Ben-Abu Y, Zhou Y, Zilberberg N, Yifrach O. Inverse coupling in leak and voltage-activated K+ channel gates underlies distinct roles in electrical signaling. Nat Struct Mol Biol. 2009;16:71–79. [PubMed: 19098918]
30. Cuello LG, Jogini V, Cortes DM, Perozo E. Structural mechanism of C-type inactivation in K+ channels. Nature. 2010;466:203–208. [PubMed: 20613835]
31. Lengyel M, Czirjak G, Enyedi P. TRESK background potassium channel is not gated at the helix bundle crossing near the cytoplasmic end of the pore. PLoS One. 2018;13:e0197622. [PubMed: 29763475]
32. Brohawn SG, Campbell EB, MacKinnon R. Domain-swapped chain connectivity and gated membrane access in a Fab-mediated crystal of the human TRAAK K+ channel. Proc Natl Acad Sci USA. 2013;110:2129–2134. [PubMed: 23341632]
33. Dong YY, Pike AC, Mackenzie A, et al. K2P channel gating mechanisms revealed by structures of TREK-2 and a complex with Prozac. Science. 2015;347:1256–1259. [PubMed: 25766236]
34. Lolicato M, Riegelhaupt PM, Arrigoni C, Clark KA, Minor DL Jr. Transmembrane helix straightening and buckling underlies activation of mechanosensitive and thermosensitive K(2P) channels. Neuron. 2014;84:1198–1212. [PubMed: 25500157]
35. Bagriantsev SN, Peyronnet R, Clark KA, Honore E, Minor DL. Multiple modalities converge on a common gate to control K2P channel function. EMBO J. 2011;30:3594–3606. [PubMed: 21765396]

36. Piechotta PL, Rapedius M, Stansfeld PJ, et al. The pore structure and gating mechanism of K2P channels. EMBO J. 2011;30:3607–3619. [PubMed: 21822218]
37. Rapedius M, Schmidt MR, Sharma C, et al. State-independent intracellular access of quaternary ammonium blockers to the pore of TREK-1. Channels (Austin). 2012;6:473–478. [PubMed: 22991046]
38. Zilberberg N, Ilan N, Goldstein SA. KCNKO: opening and closing the 2-P-domain potassium leak channel entails “C-type” gating of the outer pore. Neuron. 2001;32:635–648. [PubMed: 11719204]
39. Li J, Ostmeyer J, Cuello LG, Perozo E, Roux B. Rapid constriction of the selectivity filter underlies C-type inactivation in the KcsA potassium channel. J Gen Physiol. 2018;150:1408–1420. [PubMed: 30072373]
40. Heer FT, Posson DJ, Wojtas-Niziurski W, Nimigean CM, Berneche S. Mechanism of activation at the selectivity filter of the KcsA K(+) channel. eLife. 2017;6:e25844. [PubMed: 28994652]
41. Yellen G The moving parts of voltage-gated ion channels. Q Rev Biophys. 1998;31:239–295. [PubMed: 10384687]
42. Coonen L, Mayeur E, De Neuter N, Snyders DJ, Cuello LG, Labro AJ. The selectivity filter is involved in the U-type inactivation process of Kv2.1 and Kv3.1 channels. Biophys J. 2020;118(10):2612–2620. [PubMed: 32365329]
43. Zhou Y, Morais-Cabral JH, Kaufman A, MacKinnon R. Chemistry of ion coordination and hydration revealed by a K+ channel-Fab complex at 2.0 A resolution. Nature. 2001;414:43–48. [PubMed: 11689936]
44. Nishida M, Cadene M, Chait BT, MacKinnon R. Crystal structure of a Kir3.1-prokaryotic Kir channel chimera. EMBO J. 2007;26:4005–4015. [PubMed: 17703190]
45. Ye S, Li Y, Jiang Y. Novel insights into K+ selectivity from high-resolution structures of an open K + channel pore. Nat Struct Mol Biol. 2010;17:1019–1023. [PubMed: 20676101]
46. Tilegenova C, Cortes DM, Jahovic N, et al. Structure, function, and ion-binding properties of a K(+) channel stabilized in the 2,4-ion-bound configuration. Proc Natl Acad Sci USA. 2019;116:16829–16834. [PubMed: 31387976]
47. Tsukamoto H, Higashi M, Motoki H, et al. Structural properties determining low K(+) affinity of the selectivity filter in the TWIK1 K(+) channel. J Biol Chem. 2018;293:6969–6984. [PubMed: 29545310]
48. Jensen MO, Jogini V, Eastwood MP, Shaw DE. Atomic-level simulation of current-voltage relationships in single-file ion channels. J Gen Physiol. 2013;141:619–632. [PubMed: 23589581]
49. Miller C Coupling of water and ion fluxes in a K+-selective channel of sarcoplasmic reticulum. Biophys J. 1982;38:227–230. [PubMed: 6285998]
50. Iwamoto M, Oiki S. Counting ion and water molecules in a streaming file through the open-filter structure of the K channel. J Neurosci. 2011;31:12180–12188. [PubMed: 21865461]
51. Ando H, Kuno M, Shimizu H, Muramatsu I, Oiki S. Coupled K+-water flux through the HERG potassium channel measured by an osmotic pulse method. J Gen Physiol. 2005;126:529–538. [PubMed: 16260841]
52. Kopfer DA, Song C, Gruene T, Sheldrick GM, Zachariae U, de Groot BL. Ion permeation in K(+) channels occurs by direct Coulomb knock-on. Science. 2014;346:352–355. [PubMed: 25324389]
53. Matulef K, Komarov AG, Costantino CA, Valiyaveetil FI. Using protein backbone mutagenesis to dissect the link between ion occupancy and C-type inactivation in K+ channels. Proc Natl Acad Sci USA. 2013;110:17886–17891. [PubMed: 24128761]
54. Cuello LG, Cortes DM, Perozo E. The gating cycle of a K(+) channel at atomic resolution. eLife. 2017;6:e28032. [PubMed: 29165243]
55. Pan AC, Cuello LG, Perozo E, Roux B. Thermodynamic coupling between activation and inactivation gating in potassium channels revealed by free energy molecular dynamics simulations. J Gen Physiol. 2011;138:571–580. [PubMed: 22124115]
56. Ben Soussia I, El Mouridi S, Kang D, et al. Mutation of a single residue promotes gating of vertebrate and invertebrate two-pore domain potassium channels. Nat Commun. 2019;10:787. [PubMed: 30770809]

57. Diaz-Franulic I, Sepulveda RV, Navarro-Quezada N, Gonzalez-Nilo F, Naranjo D. Pore dimensions and the role of occupancy in unitary conductance of Shaker K channels. J Gen Physiol. 2015;146:133–146. [PubMed: 26216859]
58. Roller A, Natura G, Bihler H, Slayman CL, Bertl A. Functional consequences of leucine and tyrosine mutations in the dual pore motifs of the yeast K(+) channel, Tok1p. Pflugers Arch. 2008;456:883–896. [PubMed: 18421473]
59. Schewe M, Nematian-Ardestani E, Sun H, et al. A non-canonical voltage-sensing mechanism controls gating in K2P K(+) channels. Cell. 2016;164:937–949. [PubMed: 26919430]
60. Ma XY, Yu JM, Zhang SZ, et al. External Ba2+ block of the two-pore domain potassium channel TREK-1 defines conformational transition in its selectivity filter. J Biol Chem. 2011;286:39813–39822. [PubMed: 21965685]
61. Labro AJ, Cortes DM, Tilegenova C, Cuello LG. Inverted allosteric coupling between activation and inactivation gates in K(+) channels. Proc Natl Acad Sci USA. 2018;115:5426–5431. [PubMed: 29735651]
62. Cuello LG, Jogini V, Cortes DM, et al. Structural basis for the coupling between activation and inactivation gates in K(+) channels. Nature. 2010;466:272–275. [PubMed: 20613845]
63. Lopez BJ, Hoshi T, Heinemann SH, Aldrich RW. Effects of external cations and mutations in the pore region on C-type inactivation of Shaker potassium channels. Receptors Channels. 1993;1:61–71. [PubMed: 8081712]
64. Demo SD, Yellen G. Ion effects on gating of the Ca(2+)-activated K+ channel correlate with occupancy of the pore. Biophys J. 1992;61:639–648. [PubMed: 1504240]
65. Berneche S, Roux B. A gate in the selectivity filter of potassium channels. Structure. 2005;13:591–600. [PubMed: 15837197]
66. Matulef K, Annen AW, Nix JC, Valiyaveetil FI. Individual ion binding sites in the K(+) channel play distinct roles in C-type inactivation and in recovery from inactivation. Structure. 2016;24:750–761. [PubMed: 27150040]
67. Zheng J, Sigworth FJ. Selectivity changes during activation of mutant Shaker potassium channels. J Gen Physiol. 1997;110: 101–117. [PubMed: 9236204]
68. Brettmann JB, Urusova JC, Valiyaveetil FI. Individual Henzler-Wildman KA. Role of protein dynamics in ion selectivity and allosteric coupling in the NaK channel. Proc Natl Acad Sci USA. 2015;112:15366–15371. [PubMed: 26621745]
69. Thompson AN, Kim I, Panosian TD, Iverson TM, Allen TW, Nimigean CM. Mechanism of potassium-channel selectivity revealed by Na(+) and Li(+) binding sites within the KcsA pore. Nat Struct Mol Biol. 2009;16:1317–1324. [PubMed: 19946269]
70. Jiang YX, MacKinnon R. The barium site in a potassium channel by X-ray crystallography. J Gen Physiol. 2000;115:269–272. [PubMed: 10694255]
71. Morais-Cabral JH, Zhou Y, MacKinnon R. Energetic optimization of ion conduction rate by the K+ selectivity filter. Nature. 2001;414:37–42. [PubMed: 11689935]
72. Bichet D, Grabe M, Jan YN, Jan LY. Electrostatic interactions in the channel cavity as an important determinant of potassium channel selectivity. Proc Natl Acad Sci USA. 2006;103: 14355–14360. [PubMed: 16983069]
73. Flynn GE, Zagotta WN. Conformational changes in S6 coupled to the opening of cyclic nucleotide-gated channels. Neuron. 2001;30:689–698. [PubMed: 11430803]
74. Aryal P, Abd-Wahab F, Bucci G, Sansom MS, Tucker SJ. A hydrophobic barrier deep within the inner pore of the TWIK-1 K2P potassium channel. Nat Commun. 2014;5:4377. [PubMed: 25001086]
75. Jia Z, Yazdani M, Zhang G, Cui J, Chen J. Hydrophobic gating in BK channels. Nat Commun. 2018;9:3408. [PubMed: 30143620]

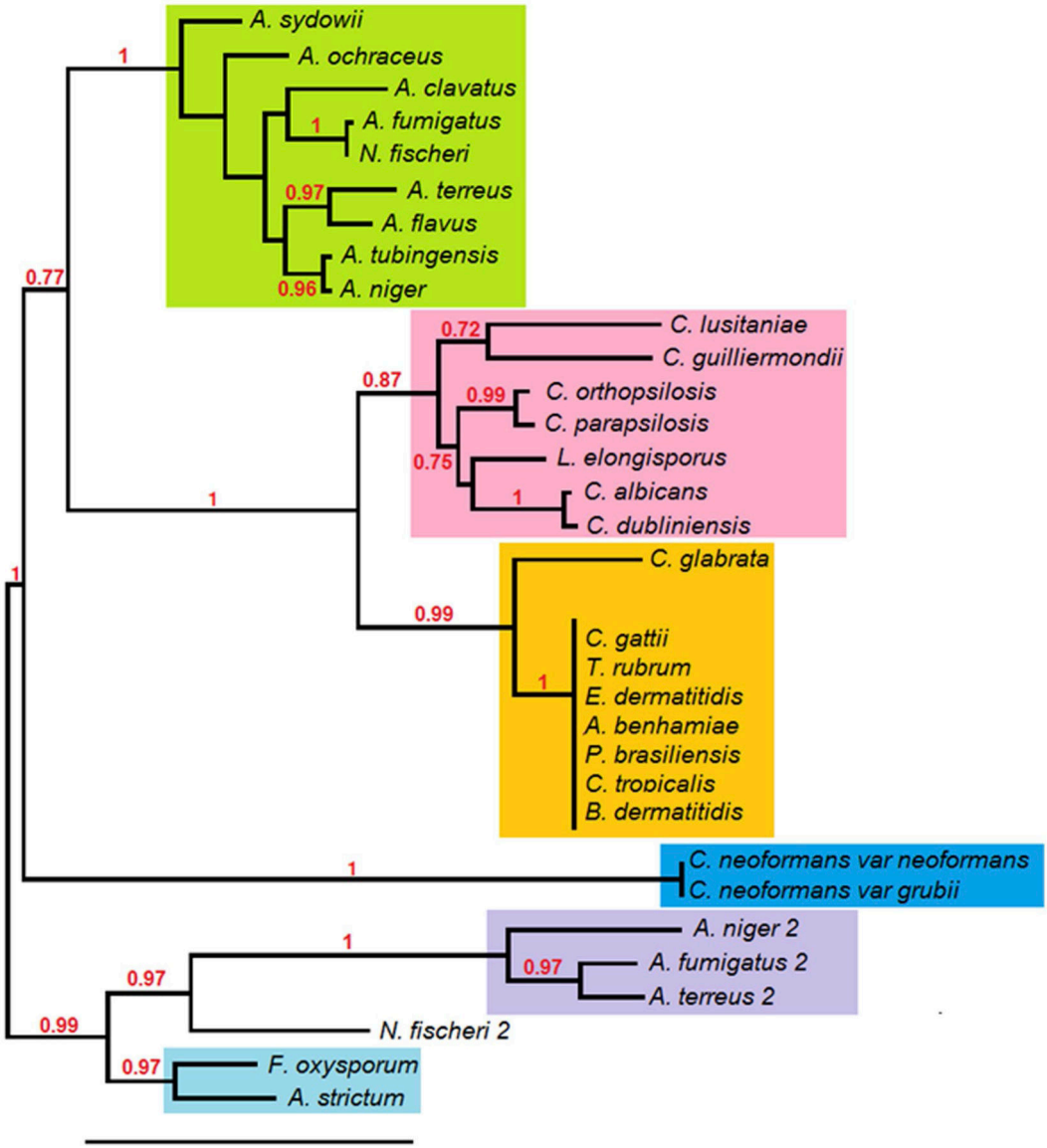

FIGURE 1.

Evolutionary relationships of TOK channels from human pathogenic fungi. Phylogram showing the inferred relationships between human pathogenic TOK channel sequences derived using MUSCLE v3.7 (default settings), GBLOCKS (default settings), PhyML v3.0 (bootstrapping at 100, substitution model WAG: protein), and TreeDyn (default settings). Branch numbers of > 0.7 are shown. Protein accession numbers are shown in the parentheses: *Cryptococcus neoformans var neofor*mans (AAW41680), *Cryptococcus neoformans var grubii* (AFR93513), *Aspergillus clavatus* (CADACLAP00002591), *Aspergillus fumigatus* (CADAFUBP00001352), *Aspergillus terreus* (CADATEAP00004105), *Aspergillus flavus* (KJJ35721), *Fusarium oxysporum* (EWZ42763), *Candida lusitaniae* (EEQ36135), *Candida guilliermondii* (EDK37268), *Candida orthopsilosis* (CCG23832), *Candida parapsilosis* (CCE44439), *Lodderomyces elongisporus* (EDK46102), *Candida albicans* (KGT68297), *Candida dubliniensis*

(CAX41959), *Candida glabrata* (KTB04901), *Cryptococcus gattii* (KIS00879), *Trichophyton rubrum* (EZF38429), *Exophiala dermatitidis* (EHY60353), *Arthroderma benhamiae* (EFE29621), *Paracoccidioides* brasiliensis (KGY15597), *Candida tropicalis* (EER35366), *Blastomyces* dermatitidis (EGE81330), *Aspergillus sydowii* (58882), *Aspergillus tubingensis* (105220), *Aspergillus strictum* (1313282), *Neosartorya fischeri* (EAW22434), *Aspergillus niger* (CAK40338), *Aspergillus fumigatus* (2), *Aspergillus terreus* (2) (XP001218595), *Neosartorya fischeri* (2) (EAW21794), *Aspergillus niger* (2) (CAK41706)

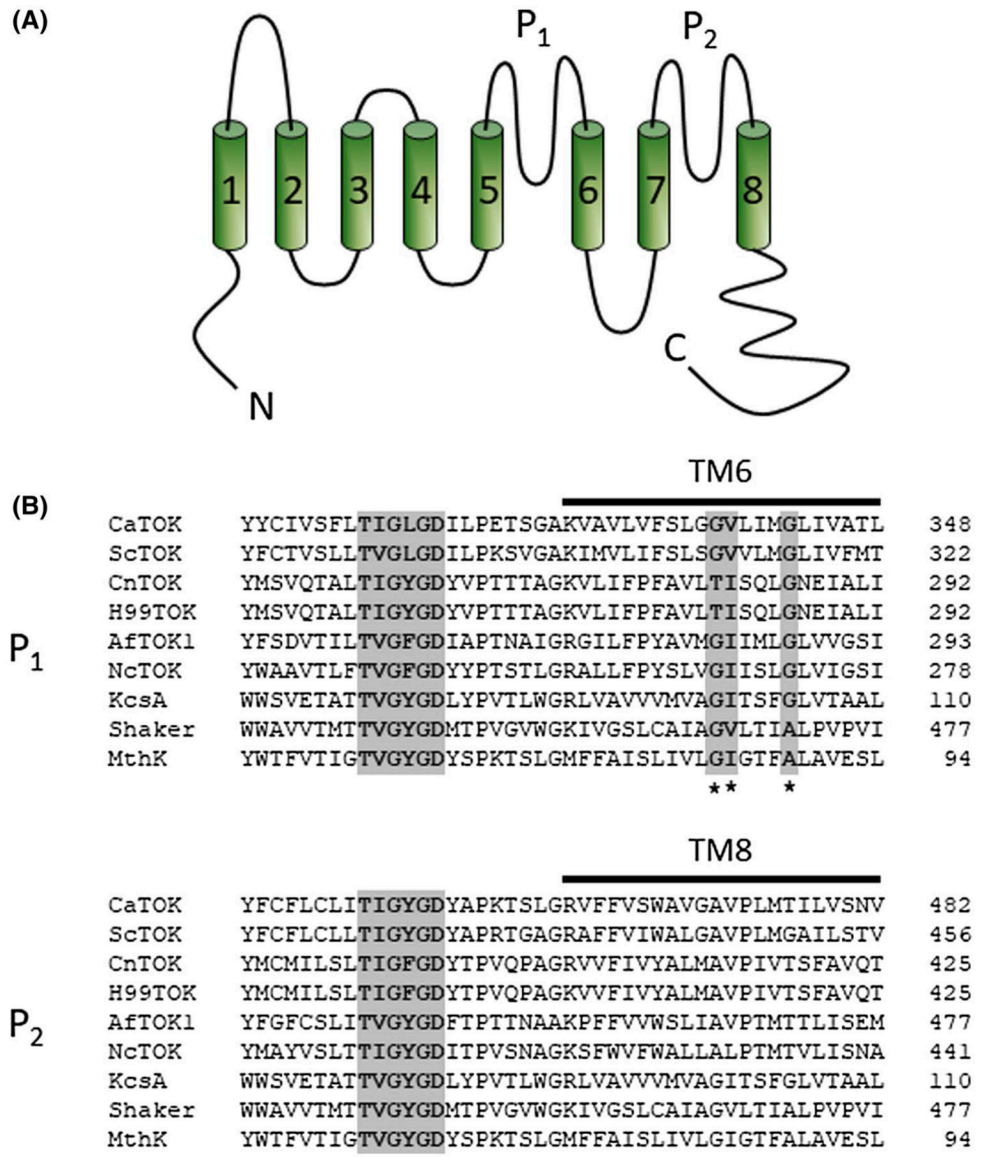

FIGURE 2.

Pore region alignment of cloned TOK channels with other known potassium channel subtypes. Alignments were generated using ClustalW 2.0 as per the materials and methods from cloned TOK channels and other potassium channel subtypes of known structure. A, Deduced topology of TOK channel homologues based on hydropathy profile analysis predicting eight putative transmembrane domains flanking two pore-forming domains with intracellular N- and C-termini. B, Sequence alignment of pore regions (P_1, upper and P_2, lower) and following transmembrane domain (TM6 or TM8, respectively) of all cloned, functional TOK channels alongside KcsA, *Shaker,* and MthK. Grey shaded area corresponds to the signature residues of the K^+ channel selectivity sequence (TXGXGD). (*) indicates location of sites identified in CaTOK and ScTOK that allow inward current

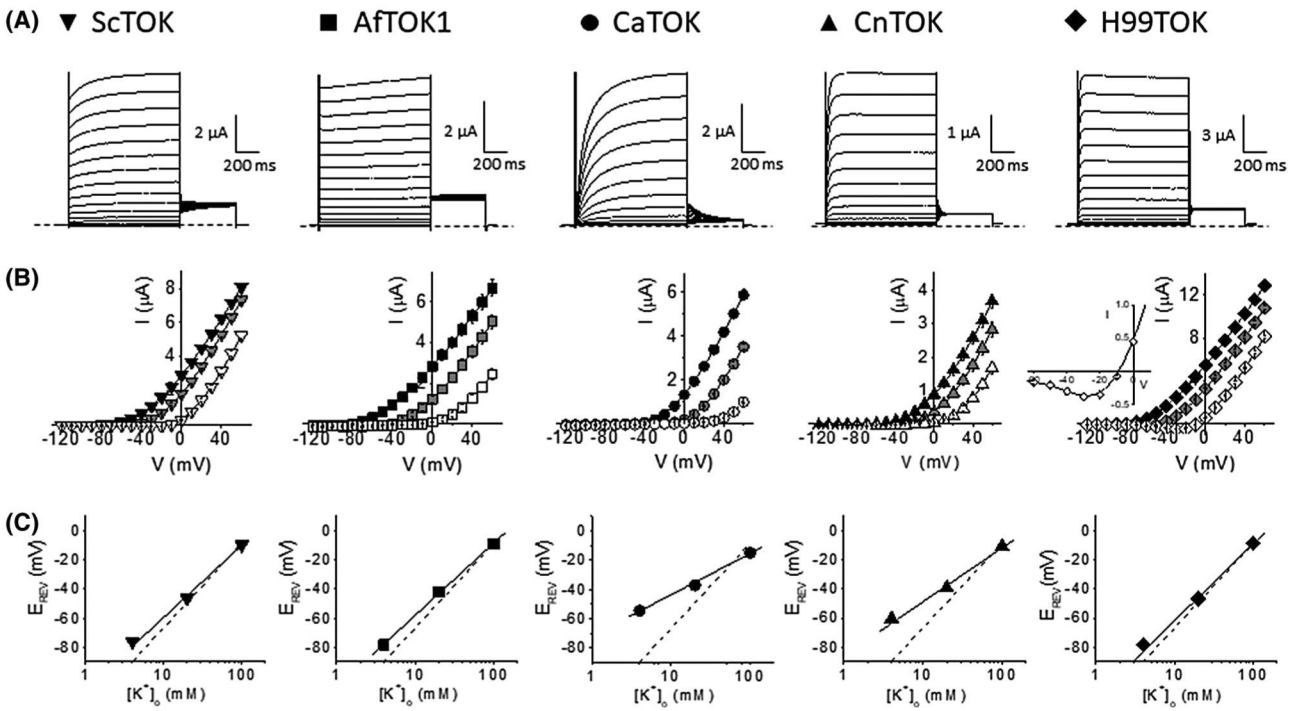

FIGURE 3.

Cloned TOK channels generate characteristic outwardly rectifying currents but with varying gating phenotypes and ion selectivity. Cloned wild type TOK channels were expressed in *Xenopus laevis* oocytes and ionic currents recorded by two-electrode voltage clamp 24 hours post injection as described in the materials and methods. Oocyte membrane potential was held at −80 mV and step depolarized from −120 mV to +60 mV in 10 mV steps for 1 seconds followed by a tail step to −30 mV for 0.5 seconds. All data are displayed as mean ± SEM (n = 4–30). Measured values are noted in the text and listed in Table 1. A, Exemplar current traces from oocytes expressing ScTOK, AfTOK1, CaTOK, CnTOK, and H99TOK, recorded in 4 mM external K^+ solution. B, Mean current-voltage (I-V) relationships taken from steady-state currents in the presence of differing concentrations of extracellular K^+; 4 mM (black symbols), 20 mM (grey symbols), and 100 mM (white symbols) shown underneath their corresponding exemplar traces in (A). H99 (*inset*); magnified view of I-V curve in 100 mM K^+ reveals small inward currents at potentials below E_K C, Plots showing relationship between current reversal potential (E_{REV}) and extracellular K^+ concentration ($[K^+]_o$) for TOK channels shown in (A) underneath their corresponding IV curves in (B). Dashed line represents Nernstian theoretical linear relationship of E_K with changing $[K^+]_o$ as calculated using the Nernst equation assuming $[K^+]_i$ is 140 mM (slope = −58.2 mV)

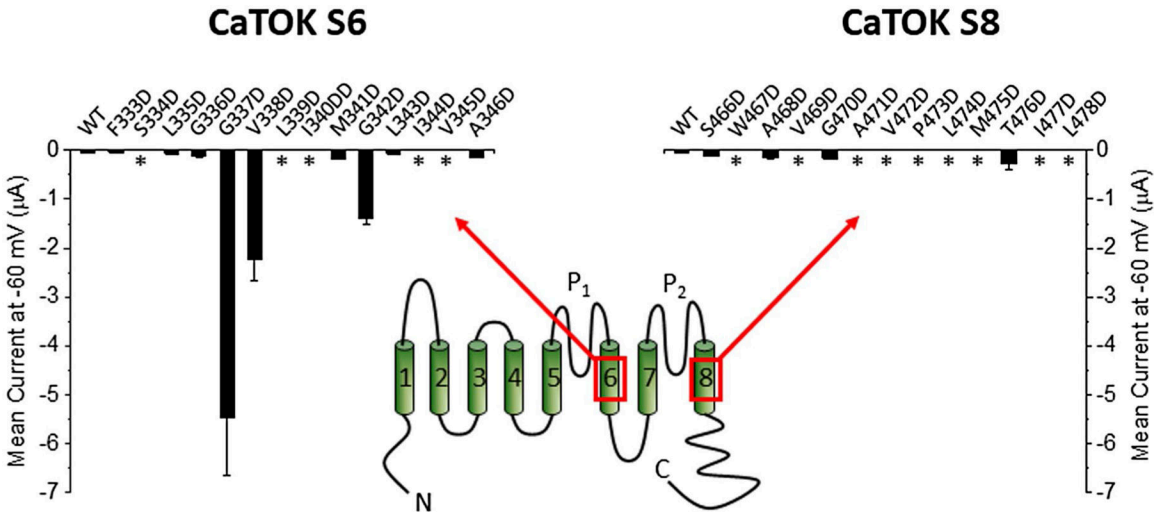

FIGURE 4.

Aspartate scan of CaTOK S6 and S8 transmembrane domains reveals three sites in S6 that permit inward current flux. Bar graphs showing mean inward current magnitude in wild type CaTOK and aspartate mutants in S6 (left) and S8 (right) measured at −60 mV with 100 mM RbCl in the bath (n = 4–16). Large inward currents were seen in G337D, V338D, and G342D. (*) indicates sites were no functional expression was observed after 72 hours expression. Inset shows the relative position of mutated sites

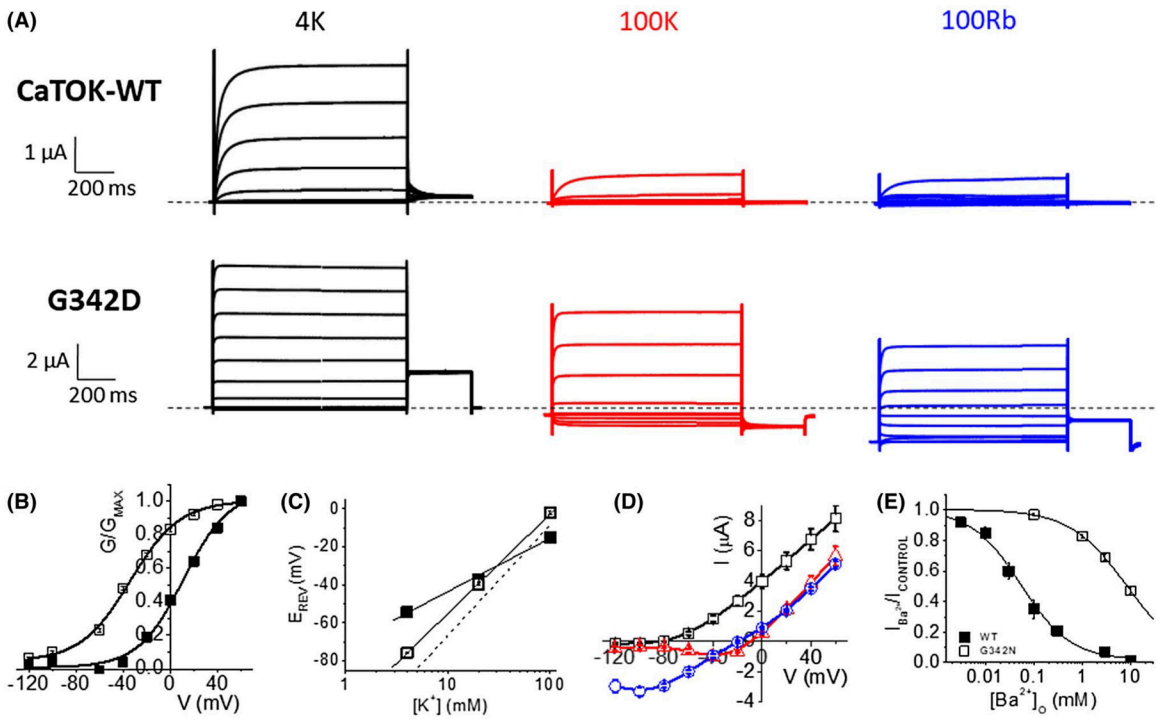

FIGURE 5.

CaTOK-G342D passes inward currents in high external K^+ or Rb^+ and has enhanced K^+ selectivity compared to wild type channels. Wild type (WT) mutant (G342D) CaTOK channels were expressed in *Xenopus laevis* oocytes and ionic currents recorded by two-electrode voltage clamp 24 hours post injection as described in the materials and methods. Oocyte membrane potential was held at −80 mV and step depolarized from −120 mV to +60 mV in 10 mV steps for 1 seconds followed by a tail step to −30 mV for 0.5 seconds. All data are displayed as mean ± SEM. Measured values are noted in the text and listed in Table 3. A, Exemplar current traces from oocytes expressing wild-type CaTOK (upper row) and the mutant CaTOK-G342D (lower row) recorded in bath solutions containing 4 mM K^+, 100 mM K^+ or 100 mM Rb^+ as indicated. Dashed line signifies baseline. B, Normalized mean conductance-voltage (G-V) relationships for wild-type CaTOK (filled squares, n = 16) and the mutant CaTOK-G342D (open squares n = 7). Conductance values were derived by dividing the steady-state current by the driving force (as stated in Methods). Each data set was fitted with a single Boltzmann function (solid curves). C, Linear plots showing relationship between current reversal potential (E_{REV}) and extracellular K^+ concentration ($[K^+]_o$) for wild-type CaTOK (filled squares) and mutant CaTOK-G342D (open squares). Dashed line represents Nernstian theoretical linear relationship of E_K with changing $[K^+]_o$ as calculated using the Nernst equation assuming $[K^+]_i$ is 140 mM (slope = −58.2 mV). D, Mean current-voltage (I-V) relationships taken from CaTOK-G342D steady-state currents in the presence of differing concentrations of extracellular K^+; 4 mM (open squares), 100 mM (open triangles) and 100 mM Rb^+ (open circles). E, Mean barium concentration-response relationships for wild-type CaTOK (filled squares, n = 6) and mutant CaTOK-G342N (open squares, n = 5). Each data set was fitted with a single Boltzmann function (solid curves)

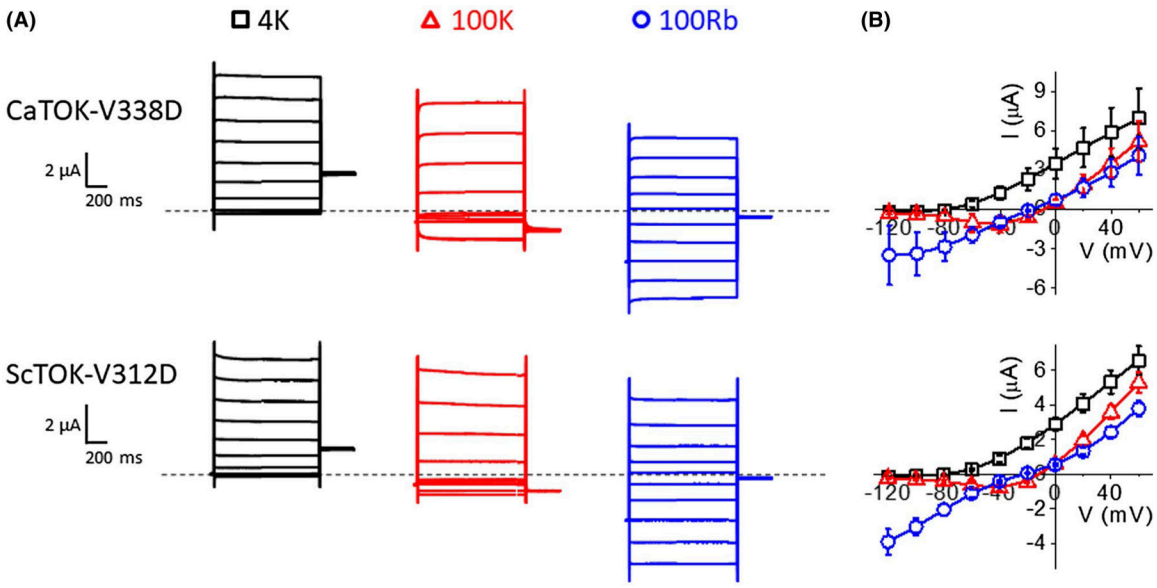

FIGURE 6.

Mutation to a second site four residues proximal to CaTOK-G342 also breaks rectification gating in both CaTOK and ScTOK channels. Wild type (WT) mutant channels were expressed in *Xenopus laevis* oocytes and ionic currents recorded by two-electrode voltage clamp 24 hours post injection as described in the materials and methods. Oocyte membrane potential was held at −80 mV and stepped to test potentials between −120 mV and +60 mV in 10 mV increments for 1 seconds followed by a voltage step to −30 mV for 500 ms before returning to the holding potential (0.1 Hz). Data are displayed as mean ± SEM. A, Exemplar current traces from oocytes expressing CaTOK-V338D (upper traces) and the analogous mutant ScTOK-V312D (lower traces) recorded in bath solutions containing 4 mM K^+, 100 mM K^+, or 100 mM Rb^+ as indicated. B, Mean current-voltage (I-V) relationships taken from steady-state currents shown in A (n = 5–6)

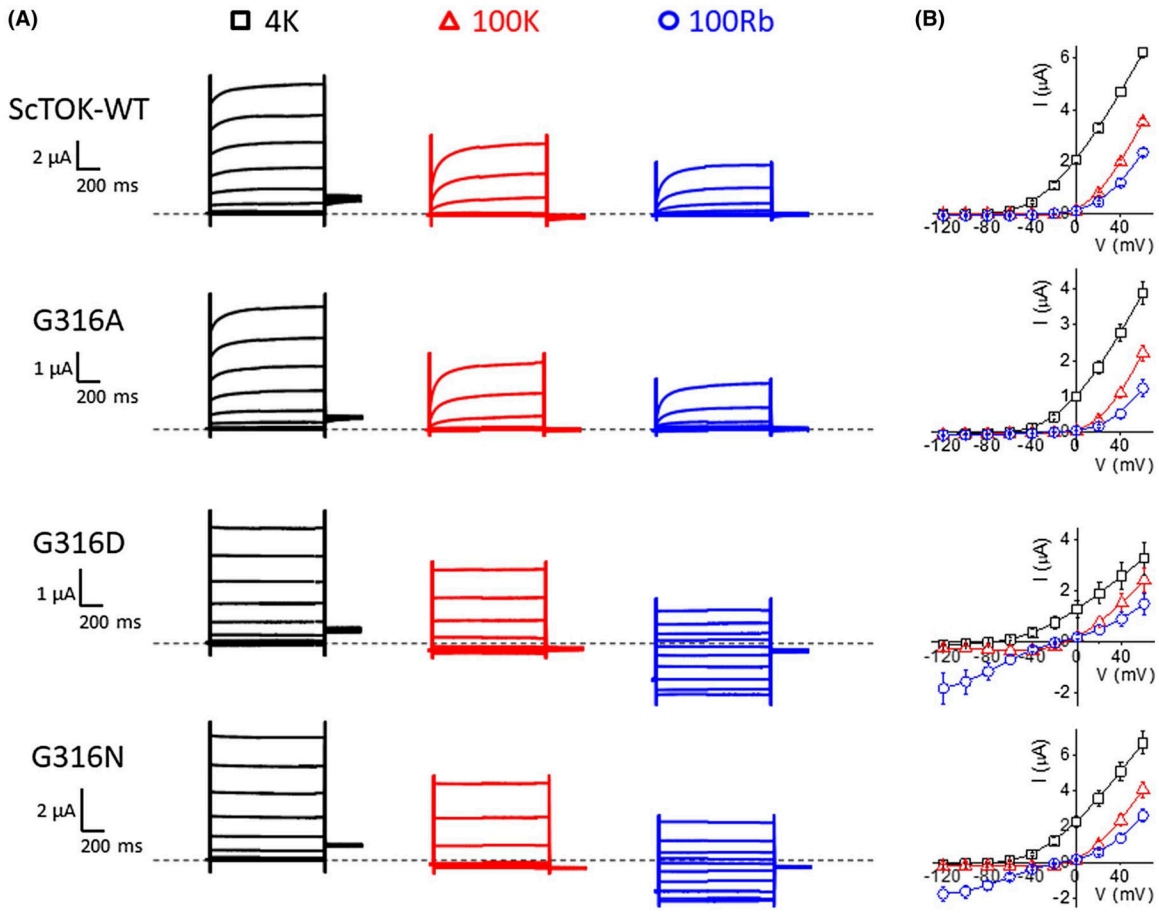

FIGURE 7.

Mutation to the CaTOK-G342 equivalent site in ScTOK generates inward current. Wild type (WT) mutant (G316) ScTOK channels were expressed in *Xenopus laevis* oocytes and ionic currents recorded by two-electrode voltage clamp 24 hours post injection as described in the materials and methods. Oocyte membrane potential was held at −80 mV and step depolarized from −120 mV to +60 mV in 10 mV steps for 1 seconds followed by a tail step to −30 mV for 0.5 seconds. All data are displayed as mean ± SEM (n = 4–6). A, Exemplar current traces from oocytes expressing wild-type ScTOK, and the mutants ScTOK-G316A, G316D, and G316N (top to bottom) recorded in bath solutions containing 4 mM K^+, 100 mM K^+, or 100 mM Rb^+ as indicated. Dashed line signifies baseline. B, Corresponding mean current-voltage (I-V) relationships taken from steady-state currents shown in A, in in bath solutions containing 4 mM K^+ (open squares), 100 mM K^+ (open triangles), or 100 mM Rb^+ (open circles)

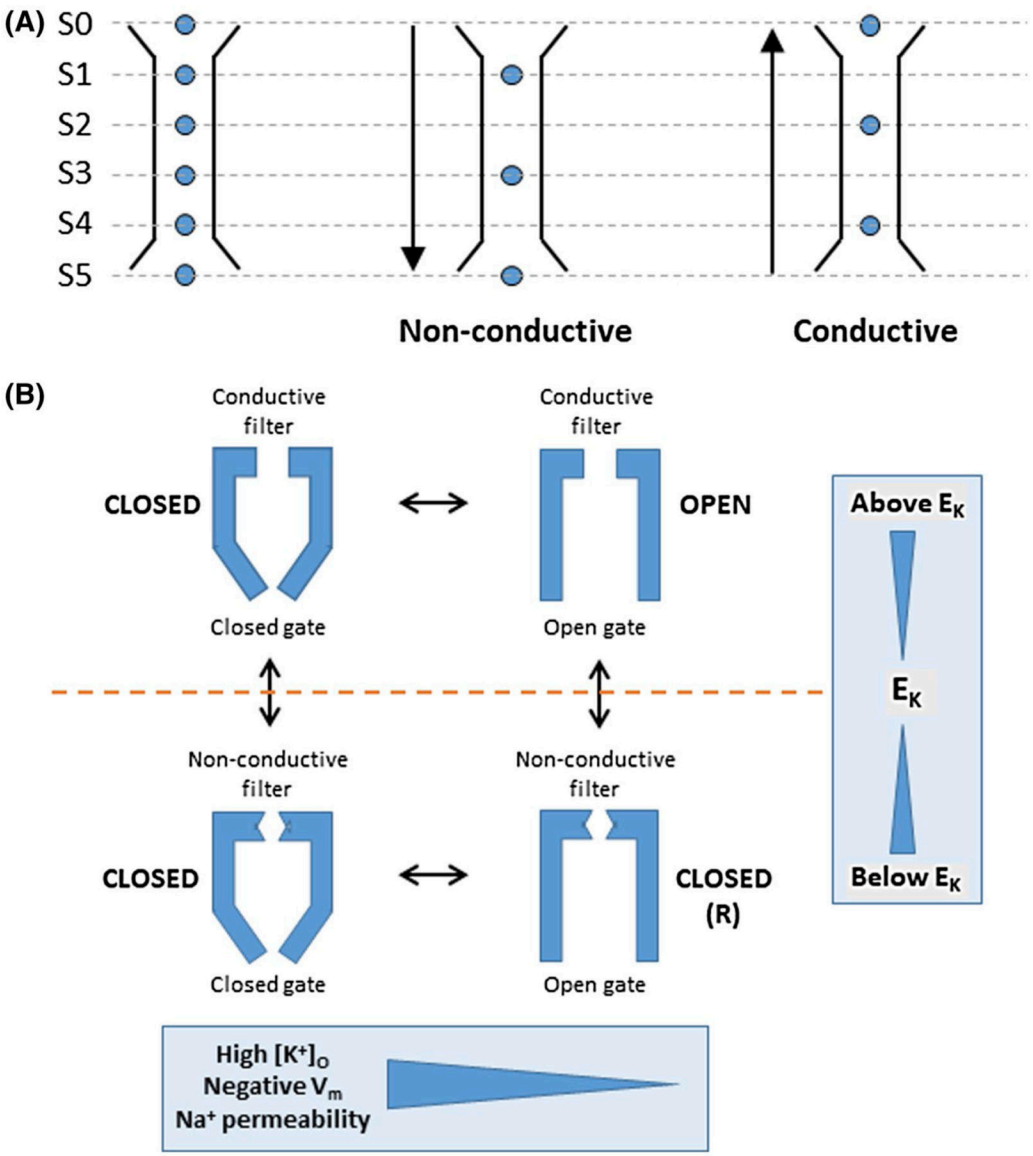

FIGURE 8.

Models illustrating proposed mechanism of TOK outward rectification and gating transitions. A, Schematic illustrating ion occupancy along the TOK channel conduction pathway in both conducting and non-conducting states. S0 represents an external ion binding site, sites S1–4 represent the four binding sites of the channel filter and S5 represents an internal cavity site below the filter. Arrows indicate the driving force for ion movement. B, Simplified gating model illustrating the various states of an open and closed TOK channel with respect to the position of the internal gate and the conductivity of the filter. Double arrows indicate ability to transition between different states

TABLE 1.

TOK channel biophysical parameters

TOK channel	GHK predicted Erev (mV)	Threshold activation (E_K −90 mV) (mV)	ΔE_{REV} per 10-fold change $[K^+]_o$ (mV)	V½ (mV)	Instant/ peak current at 40 mV in 4 mM KCl and (100 mM K^+)	Time-dependent activation at +40 mV in 4 mM K^+ and (100 mM K^+)			τ deactivation at −30 mV in 4 mM K^+ (ms)
						τ_{slow} (ms)	τ_{fast} (ms)	$\frac{a_f}{a_f + a_s}$	
ScTOK	−72.8	−76 ± 1.0	50 ± 1.0	−2.0 ± 2.0	0.8 ± 0.02 (0.3 ± 0.02)	498 ± 60 (622 ± 83)	133 ± 12 (100 ± 10)	0.4 ± 0.04 (0.5 ± 0.04)	<5
AfTOK1	−79.9	−79 ± 1.0	50 ± 1.0	−50 ± 5.0	1.0 ± 0.01 (0.7 ± 0.03)	-	-	-	<5
H99TOK	−76.1	−79 ± 1.0	53 ± 1.0	−18 ± 2.0	0.4 ± 0.05 (0.0 ± 0.00)	12.8 ± 0.7 (22.9 ± 0.6)	3.9 ± 0.3 (6.1 ±0.08)	0.4 ± 0.02 (0.7 ± 0.01)	11.1 ± 0.3
CnTOK	−65.0	−60 ± 2.0	37 ± 1.0	14 ± 1.0	0.0 ± 0.00 (0.0 ± 0.00)	42.4 ± 3.1 (50.4 ± 8.8)	14.5 ± 1.6 (19.7 ± 3.3)	0.5 ± 0.01 (0.5 ± 0.07)	29.6 ± 1.6
CaTOK	−57.3	−54 ± 1.0	28 ± 1.0	10 ± 1.0	0.0 ± 0.00 (0.0 ± 0.00)	207 ± 16.1 (481 ± 13.3)	42.0 ± 3.7 (94.4 ±3.1)	0.6 ± 0.02 (0.5 ± 0.04)	138 ± 5.1

Legend: Data with TOK channels expressed in *Xenopus* oocytes (n = 4–30) recorded in 4 mM $[K^+]_O$ or 100 mM $[K^+]_O$ as indicated. Values represent mean ± SEM. V½, voltage of half-maximal activation; E_{REV}, reversal potential; a_f and a_S, amplitudes of fast and slow components of activation, respectively; $[K^+]_O$, extracellular potassium concentration. For comparison, the value for ΔE_{REV} per 10-fold change in $[K^+]_O$ for a channel that is ideally selective for potassium is 58.2 mV under these conditions. GHK predicted values calculated using the GHK equation, based on permeability ratios from nearly bi-ionic reversal potential measurements in Table 2.

TABLE 2

Relative ionic selectivity for cloned fungal TOK channels

		ScTOK	AfTOKl	CaTOK	CnTOK	H99TOK
K+	P_k/P_k	1.0	1.0	1.0	1.0	1.0
Rb+	P_{Rb}/P_K	0.66 ± 0.01	0.61 ± 0.11	0.85 ± 0.05	0.69 ± 0.03	0.55 ± 0.01
Cs+	P_{cs}/P_k	0.24 ± 0.03	0.07 ± 0.00	0.28 ± 0.02	0.20 ± 0.02	0.08 ± 0.01
Na+	P_{Na}/P_K	0.04 ± 0.01	0.02 ± 0.00	0.11 ± 0.01	0.07 ± 0.01	0.03 ± 0.00
Li+	P_{Li}/P_k	0.04 ± 0.01	0.01 ± 0.00	0.05 ± 0.01	0.11 ± 0.02	0.03 ± 0.00

Macroscopic reversal potentials and ion selectivity of AfTOK1, CaTOK, CnTOK, H99TOK, and ScTOK channels expressed as permeability rations (P_X/P_K) after adjustment for liquid junction potentials. Values represent mean ± SEM for n = 6–10 oocytes. P_X/P_K was determined from nearly bi-ionic reversal potential measurements where 100 mM $[K^+]_o$ was replaced with 100 mM of the indicated monovalent cation, according to the formula: $\frac{p_x}{p_k} = e\left(\frac{\Delta \text{Erev} \,.\, \text{F}}{\text{RT}}\right)$

TABLE 3.

Summary of CaTOK-G342 mutant biophysical characteristics.

Data were taken from CaTOK-G342 mutant channels expressed in *Xenopus* oocytes recorded in 4 mM $[K^+]_o$ as detailed in the Methods. Values represent mean ± SEM. Abbreviations; V½, voltage of half maximal activation, E_{REV}, reversal potential, a_f and a_s, amplitudes of fast and slow components of activation respectively, $[K^+]_o$, extracellular potassium concentration. For comparison, the Nernstian value for $\Delta E_{REV}/\log\Delta [K^+]_o$ was calculated to be 58.2 mV for a potassium selective channel. Values for wild type CaTOK have been taken from Table 1 to allow direct comparison with mutant channels. CaTOK-G342K was non-functional (n.f.) and dash (-) indicates parameter could not be measured.

CaTOK Mutant (*n*)	Threshold for activation in (mV) (~E_k = −80)	$\Delta E_{REV}/\log\Delta [K^+]_o$ (mV)	V½ (mv)	Instant/peak current at + 40 mV in 4 mM K^+	Time-dependent activation at + 40 mV			τ deactivation at −30 mV (ms)
					τ_{slow} (ms)	τ_{fast} (ms)	$\frac{a_f}{a_f + a_s}$	
WT 16	**−54 ± 1.0**	**28 ± 1.0**	**10 ± 0.8**	**0.08 ± 0.01**	**207 ± 16**	**42 ± 4**	**0.6 ± 0.0**	**138 ± 5**
G342**A** (5)	−61 ± 0.7	34 ± 0.6	5 ± 0.8	0.17 ± 0.01	98 ± 5	20 ± 1	0.6 ± 0.0	81 ± 2
G342**C** (5)	−39 ± 2.1	19 ± 1.6	33 ± 1.7	0.08 ± 0.02	569 ± 36	132 ± 8	0.6 ± 0.0	174 ± 6
G342**D** (7)	−78 ± 0.7	52 ± 1.0	−50 ± 2.8	0.87 ± 0.04	16 ± 3	7 ± 1	0.4 ± 0.1	-
G342**E** (5)	−68 ± 2.0	46 ± 2.1	−21 ± 1.2	0.70 ± 0.02	206 ± 18	18 ± 1	0.7 ± 0.0	16 ± 1
G342**F** (7)	−59 ± 0.4	23 ± 1.5	17 ± 1.3	0.05 ± 0.00	1088 ± 86	234 ± 19	0.4 ± 0.0	1707 ± 253
G342**K** (X)	n.f.	n.f.	n.f.	n.f.	n.f.	n.f.	n.f.	n.f.
G342**L** (6)	−48 ± 1.5	23 ± 5.1	29 ± 1.4	0.04 ± 0.00	770 ± 75	237 ± 32	0.3 ± 0.0	503 ± 14
G342**N** (6)	−79 ± 0.3	52 ± 0.1	−64 ± 5.7	0.99 ± 0.00	-	-	-	-
G342**Q** (6)	−80 ± 1.2	49 ± 1.1	−27 ± 2.4	0.93 ± 0.01	19 ± 1	8 ± 2	0.3 ± 0.1	-
G342**S** (5)	−69 ± 1.8	36 ± 1.7	−1 ± 1.2	0.25 ± 0.03	78 ± 2	16 ± 1	0.6 ± 0.0	83 ± 2